Archives of Hydro-Engineering and Environmental Mechanics
Vol. 48 (2001), No. 1, pp. 35–61

Two-dimensional Shallow Water Model for Rapidly and Gradually Varied Flow

Michał Szydłowski

Technical University of Gdańsk, Faculty of Hydro and Environmental Engineering
ul. Narutowicza 11/12, 80-952 Gdańsk, Poland

(Received September 19, 2000; revised February 06, 2001)

Abstract

The numerical solution of full shallow water equations (SWE) including the eddy viscosity terms is presented. In the first part of the paper the solution of the homogeneous part of SWE for discontinuous, rapidly varied flow is reported. The method presented here is based on Roe idea of numerical fluxes of mass and momentum. The numerical solution of SWE on unstructured, triangular mesh is reported and the influence of geometry approximation is examined. The imposing of the boundary condition on a triangular numerical mesh is described in detail. The consistent with finite volume method (FVM) approximation of the viscous part of SWE is presented. The procedure similar to the finite element method (FEM) is used to calculate the function derivatives inside the finite volumes. The specific difficulties of source terms numerical integration are studied and some methods to avoid these problems are presented. To integrate the bottom friction term the splitting technique is implemented. The computed results are compared to analytical solution of Saint- Venant equations, experimental data and results available in the literature. Good agreement between these results is observed.

1. Introduction

The shallow water equations (SWE) are the system of partial differential equations describing twodimensional, integrated along depth, free surface water flow. This set of equations can be derived from continuity and Navier-Stokes equations (Sawicki 1998). Unfortunately, an analytical solution of SWE, in most real cases, does not exist and they must be solved by numerical methods. A lot of classical methods for solving the water flow equations are known and successfully applied. Generally they are based on the finite difference method (FDM) (Abbott 1979) and finite element method (FEM) (Sa Da Costa et al. 1986; Szymkiewicz 1991, 1995). Usually, these methods produce adequate results for continuous, gradually varied flow. The same schemes are often useless when discontinuities (i.e. hydraulic jumps) appear. There usually exist some result oscillations near the

discontinuity and modification of the methods is needed to avoid these computational difficulties. The unphysical effects are the result of numerical diffusivity of the schemes. The special versions of the FEM scheme for discontinuous flow were presented by Katopodes (1984) and Arnold (1996). These modified schemes produce adequate results but unfortunately their implementation is relatively complicated.

Recently several methods for handling the flow discontinuities were developed. The basic calculation techniques are known as "shock-fitting methods" and "schemes with artificial viscosity" (Cunge et al. 1980). In the last two decades up-wind methods with flux vector-splitting technique (Steger and Warming 1981) and Riemann problem solution (Glaister 1993, Nujic 1995, Ambrosi 1995) were intensively investigated and applied in hydrodynamics. The method based on Roe's (1981) solution of the approximate the Riemann problem for one- and two-dimensional free surface water flow equations was also studied and reported by Szydłowski (1998). Previously, the presented scheme was adequate to calculate rapidly varied flow in regions where the water flow changes from subcritical to supercritical and vice versa. That numerical scheme handled discontinuity properly and was of second-order accuracy in space and time in smooth flow regions. However, the model presented previously was devoid of diffusion of momentum terms. Of course, for accurate description of both rapidly and gradually varied flow, the SWE should contain that term as well as the bottom friction and gravity terms. Previously, the flow equations were approximated by finite volume method (FVM) but the approximation was limited to rectangular, structured mesh. This approach produced adequate results when geometry of calculation domain was regular. Unfortunately, for complex geometry the numerical results of flow simulation were unsatisfactory.

The present paper reports on the construction of numerical model based on full SWE approximated by FVM on unstructured, triangular mesh. In order to solve SWE the inviscid fluxes at the cell-interfaces are calculated in accordance with Roe linearization of the Riemann problem. To estimate the viscid fluxes between two cells (finite volumes) function gradients at cell-interfaces are needed. They are calculated in a manner similar to FEM procedure. Because of numerical difficulties, existing due to abrupt bathymetry and supercritical flow, some special techniques of source term integration are presented. In the last section of the paper some numerical tests are studied. For rapidly varied flow numerical results are compared with analytical solutions of onedimensional SWE and experimental data. The physical modelling took place in the Hydraulic Laboratory of the Catholic University of Louvain, Belgium. The experimental work was carried out by Prof. Ives Zech Research Group within the framework of "Concerted Action on Dam-Break Modelling" (CADAM). In order to validate viscid terms of SWE the numerical test presented by Stelling (1984) is examined.

2. Finite Volume Discretization of SWE on Triangular, Unstructured Mesh

The system of SWE with viscid terms in conservative form (Abbott 1979) can be written as

$$\frac{\partial \mathbf{U}}{\partial t} + \frac{\partial \mathbf{E}}{\partial x} + \frac{\partial \mathbf{M}}{\partial x} + \frac{\partial \mathbf{G}}{\partial y} + \frac{\partial \mathbf{N}}{\partial y} + \mathbf{S} = 0 \tag{1}$$

where

$$\mathbf{U} = \begin{pmatrix} h \\ uh \\ vh \end{pmatrix}, \mathbf{E} = \begin{pmatrix} uh \\ u^2h + 0.5g\,h^2 \\ uvh \end{pmatrix}, \mathbf{G} = \begin{pmatrix} vh \\ uvh \\ v^2h + 0.5g\,h^2 \end{pmatrix} \tag{2a, b, c}$$

$$\mathbf{M} = \begin{pmatrix} 0 \\ -\nu h \frac{\partial u}{\partial x} \\ -\nu h \frac{\partial v}{\partial x} \end{pmatrix}, \mathbf{N} = \begin{pmatrix} 0 \\ -\nu h \frac{\partial u}{\partial y} \\ -\nu h \frac{\partial v}{\partial y} \end{pmatrix}, \mathbf{S} = \begin{pmatrix} 0 \\ -g\,h\,(S_{0x} - S_{fx}) \\ -g\,h\,(S_{0y} - S_{fy}) \end{pmatrix} \tag{2d, e, f}$$

In this system of equations h represents water depth, u and v are the depth-averaged components of velocity in x and y direction, respectively, S_{0x} and S_{0y} denote the bed slope terms, S_{fx} and S_{fy} are the bottom friction terms, g is the acceleration due to gravity and ν is the eddy viscosity coefficient. The bottom friction can be described by the Manning formula (Tan 1992):

$$S_{fx} = \frac{n^2 u \sqrt{u^2 + v^2}}{h^{4/3}}, S_{fy} = \frac{n^2 v \sqrt{u^2 + v^2}}{h^{4/3}}. \tag{3a, b}$$

Equation (1) can be rewritten as

$$\frac{\partial \mathbf{U}}{\partial t} + div\mathbf{F} + div\mathbf{D} + \mathbf{S} = 0. \tag{4}$$

Vectors **F** and **D** in equation (4) are given as

$$\mathbf{F}\mathbf{n} = \mathbf{E}n_x + \mathbf{G}n_y, \mathbf{D}\mathbf{n} = \mathbf{M}n_x + \mathbf{N}n_y \tag{5a, b}$$

where $\mathbf{n} = (n_x, n_y)^{\mathrm{T}}$ is a unit vector.

To integrate the SWE system (4) in space, using the finite volume method, the calculation domain is discretized into set of triangular cells (Fig. 1). This kind of approximation gives an unstructured numerical mesh. Each cell is defined by its centre point and all variables are averaged and constant inside the cell.

After integration and applying the Ostrogradski-Gauss theorem (Bronsztejn and Siemiendiajew 1973) equation (4) for each triangle cell can be written as

$$\frac{\partial \mathbf{U}_i}{\partial t} \Delta A_i + \oint_{L_i} (\mathbf{F}\mathbf{n})\, dL + \oint_{L_i} (\mathbf{D}\mathbf{n})\, dL + \int_{\Delta A_i} \mathbf{S} dA = 0 \tag{6}$$

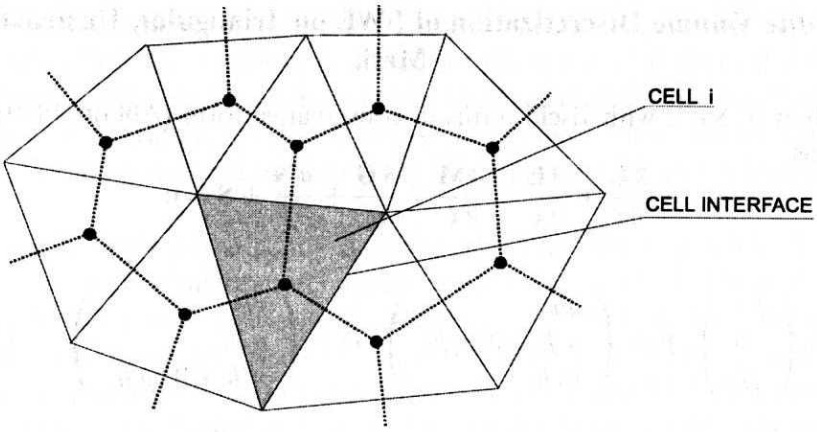

Fig. 1. Discretization of calculation domain by triangular finite volumes (cells)

where ΔA_i and L_i are the area and boundary of cell i. The first term of equation (6) represents time evolution of conserved variables over the cell. The surface integrals are total normal inviscid and viscid fluxes through the boundary of cell i, respectively. The last integral is an integral of SWE source terms. All integrals in equation (6) can be substituted by corresponding sums of three components as follows:

$$\frac{\partial \mathbf{U}_i}{\partial t}\Delta A_i + \sum_{r=1}^{3}(\mathbf{F}_r \mathbf{n}_r)\,\Delta L_r + \sum_{r=1}^{3}(\mathbf{D}_r \mathbf{n}_r)\,\Delta L_r + \sum_{r=1}^{3}\mathbf{S}_r \Delta A_r = 0 \tag{7}$$

where $\mathbf{F}_r$ and $\mathbf{D}_r$ are the numerical (computed at r^{th} cell-interface) fluxes and ΔL_r represents the cell-interface length. $\mathbf{S}_r$ and ΔA_r are the components of source terms and area of cell i assigned to r^{th} cell-interface. To simulate the free surface water flow, equations (7) must be solved inside every finite volume i. Appropriate sums are therefore necessary and a time integration scheme must be implemented.

3. Inviscid Fluxes

In order to calculate the inviscid fluxes $\mathbf{F}_r$, the solution of the approximate Riemann problem presented by Roe (1981) is used. The computation procedure is available in the literature (Glaister 1993, Ambrosi 1995, Toro 1997) and was also reported by Szydłowski (1998), hence only the bases of the computational method are presented here.

Applying the Roe idea of approximate Riemann problem solution the numerical flux at r^{th} cell-interface can be expressed as

$$\mathbf{F}_r \mathbf{n} = \frac{1}{2}(\mathbf{F}_L + \mathbf{F}_R) - \frac{1}{2}\sum_{k=1}^{3}\bar{\alpha}_k \left|\bar{\lambda}_k\right| \bar{\mathbf{r}}_k \mathbf{n}_r \tag{8}$$

where $\bar{\lambda}_k$ and $\bar{\mathbf{r}}_k$ are the eigenvalues and eigenvectors of jacobian $\mathbf{A} = \partial\mathbf{F}/\partial\mathbf{U}$. For SWE the coefficients $\bar{\alpha}_k (k = 1, 2, 3)$ equal

$$\begin{aligned}
\bar{\alpha}_1 &= \tfrac{\Delta h}{2} - \tfrac{1}{2\bar{c}}\left[\Delta(hu)\, n_x + \Delta(hv)\, n_y - \left(\bar{u}n_x + \bar{v}n_y\right)\Delta h\right], \\
\bar{\alpha}_2 &= \left[\Delta h\bar{v} - \Delta(hv)\right] n_x - \left[\Delta\bar{u} - \Delta(hu)\right] n_y, \qquad \text{(9a, b, c)} \\
\bar{\alpha}_3 &= \tfrac{\Delta h}{2} + \tfrac{1}{2\bar{c}}\left[\Delta(hu)\, n_x + \Delta(hv)\, n_y - \left(\bar{u}n_x + \bar{v}n_y\right)\Delta h\right].
\end{aligned}$$

The values of water depth $\bar{h}$ and velocity components $\bar{u}$ and $\bar{v}$ are the Roe averages and can be calculated as follows

$$\begin{aligned}
\bar{h} &= \frac{h_L + h_R}{2} \Rightarrow \bar{c} = \sqrt{g\bar{h}}, \\
\bar{u} &= \frac{\sqrt{h_L}u_L + \sqrt{h_R}u_R}{\sqrt{h_L} + \sqrt{h_R}}, \qquad \text{(10a, b, c)} \\
\bar{v} &= \frac{\sqrt{h_L}v_L + \sqrt{h_R}v_R}{\sqrt{h_L} + \sqrt{h_R}}.
\end{aligned}$$

States $\mathbf{U}_L$ and $\mathbf{U}_R$ are defined on both sides of the r^{th} cell-interface. Generally, the method proposed by Roe can be used to solve the systems of hyperbolic equations, such as Euler or Saint-Venant equations. Numerical schemes, based on the Roe idea of numerical fluxes, are adequate for discontinuous water flows. They also produce good results for rapidly varied flow due to dam-break (Szydłowski 1998).

4. Viscid Fluxes

In order to estimate the viscid fluxes $\mathbf{D}_r$, which are needed to solve equation (7), derivatives of velocity components u and v at the r^{th} cell-interface are required. For two cells i and ii (Fig. 2) the derivative of any function can be approximated by weighted average of derivatives computed inside the triangles $T1$ (vertexes i, j, k) and $T2$ (vertexes j, ii, k).

For the sake of clarity let us consider only one derivative of one velocity component $u_x = \partial u/\partial x$. If the derivatives in triangles $T1$ and $T2$ (u_x^{T1}, u_x^{T2}) are known, the averaged value at r^{th} cell-interface can be expressed as

$$u_x^r = \frac{u_x^{T1}A^{T1} + u_x^{T2}A^{T2}}{A^{T1} + A^{T2}} \qquad (11)$$

where A^{T1} and A^{T2} are the areas of triangles $T1$ and $T2$, respectively. To compute $u_x{}^r$ the values of derivatives inside both triangles are needed. They can be calculated in a manner similar to FEM with linear base functions (Zienkiewicz 1972). For instance, the value of u_x in triangle $T1$ (i, j, k) can be approximated as follows:

$$u_x^{T1} = u_i\frac{b_i}{2A^{T1}} + u_j\frac{b_j}{2A^{T1}} + u_k\frac{b_k}{2A^{T1}} \qquad (12)$$

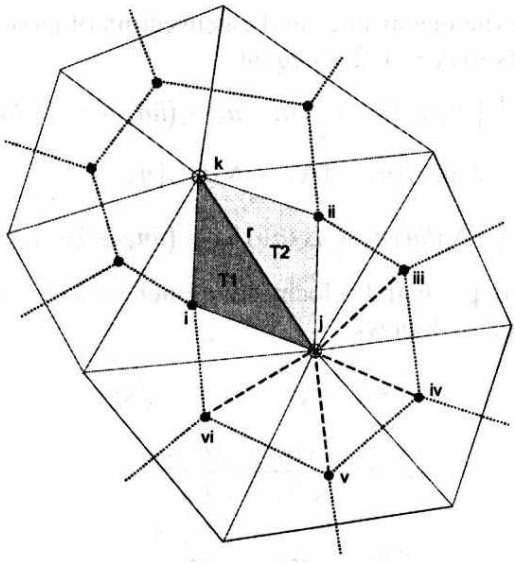

Fig. 2. Scheme for derivative calculation

where u_i, u_j and u_k are the values of velocity at nodes i, j, k, respectively. Factors $b_l (l = i, j, k)$ and c_l (needed to compute the derivatives in y direction) are equal to

$$b_i = y_j - y_k, b_j = y_k - y_i, b_k = y_i - y_j \qquad \text{(13a, b, c)}$$

$$c_i = x_k - x_j, c_j = x_i - x_k, c_k = x_j - x_i \qquad \text{(13d, e, f)}$$

where x_l and y_l (l=i, j, k) are the coordinates of the vertexes i, j, k. Unfortunately, only at node i are the velocity components known. At vertexes j and k the velocities must be approximated. They can be obtained by a distance-weighted average of cell-centre values from volumes surrounding vertexes j and k, respectively. For instance, vertex j (Fig. 2) is included into six (i, ii, iii, iv, v, vi) neighbouring cells and values of velocity from all these nodes must be taken into consideration. In a similar manner, the other derivatives of velocity components can be calculated. Finally, the viscid fluxes at r^{th} cell-interface can be calculated from (2d, e) and (5b) using approximated derivatives (11) and Roe averaged water depth (10a).

5. Source Terms

The source term vector **S** (2f) contains two sorts of elements, dependent on bottom and friction slopes, respectively. Both of them pose some numerical integration difficulties. For instance, after inconsistent implementation of the bottom slope term, some artificial (unphysical) oscillations of depth and velocity can occur (Nujic 1995, Goutal and Maurel 1997). To avoid these effects, the source term

should be up-winded in the same way as inviscid fluxes. This problem was investigated by Bermudez and Vazquez (1994). The numerical source method proposed by them for the 1D problem was also examined by Szydłowski (1998) for 2D Saint-Venant equations. Recently, the importance of bed slope approximation has been reported by Jha et al. (2000).

Applying the numerical source method, each sum component $\mathbf{S}_r$ in equation (7) can be expressed as

$$\mathbf{S}_r = \left(\mathbf{I} - |\mathbf{A}|\,\mathbf{A}^{-1}\right) \mathbf{S}\,(\mathbf{U}_L, \mathbf{U}_R, \mathbf{n}) \tag{14}$$

where $\mathbf{I}$ is the unit matrix and Roe averages (9) are used to compute the values of source terms at r^{th} cell-interface. The sum mentioned contains as many components as neighbouring cells of given volume i exist.

The second source term of SWE (bottom friction term) can be determined by the Manning formula. Generally, this approach is adequate for steady water flow, but due to no alternative method it is also used for unsteady flows, producing satisfactory results. Some difficulties appear when supercritical flow exists. Applying the Manning formula for flow with great velocity and small depth produces numerical errors. The very large value of $u^2/h^{4/3}$ type terms in equations (3a, b) usually leads to solution instability. Finally, some unexpected result oscillations destroy the computation. In order to avoid this inconvenience the splitting technique with respect to physical processes (Szymkiewicz 1993) can be applied.

The SWE system (1) can be written in another matrix form

$$\frac{\partial \mathbf{U}}{\partial t} = \mathbf{X} \tag{15}$$

where vector $\mathbf{X}$ contains all terms of equation (1) except for the time derivatives. The solution of equation (15) can be obtained by integration in time increment $\langle t,\ t+\Delta t\rangle$. The general time integration scheme, defining a new function value at numerical grid time level $n+1$,

$$\mathbf{U}^{n+1} = \mathbf{U}^n + \int_0^{\Delta t} \mathbf{X} dt \tag{16}$$

after substitution of vector $\mathbf{X}$ by the sum

$$\mathbf{X} = \mathbf{X}_{(1)} + \mathbf{X}_{(2)} \tag{17}$$

can be transformed as follows

$$\mathbf{U}^{n+1} = \mathbf{U}^n + \int_0^{\Delta t} \mathbf{X}_{(1)}\, dt + \int_0^{\Delta t} \mathbf{X}_{(2)}\, dt. \tag{18}$$

For SWE (1) the vectors $\mathbf{X}_{(1)}$ and $\mathbf{X}_{(2)}$ can be written as

$$\mathbf{X}_{(1)} = \begin{pmatrix} -\frac{\partial (uh)}{\partial x} - \frac{\partial (vh)}{\partial y} \\ -\frac{\partial (u^2h+0.5gh^2)}{\partial x} - \frac{\partial (uvh)}{\partial y} - gh\frac{\partial z_b}{\partial x} + \frac{\partial}{\partial x}\left(\nu h\frac{\partial u}{\partial x}\right) + \frac{\partial}{\partial y}\left(\nu h\frac{\partial u}{\partial y}\right) \\ -\frac{\partial (uvh)}{\partial x} - \frac{\partial (v^2h+0.5gh^2)}{\partial y} - gh\frac{\partial z_b}{\partial y} + \frac{\partial}{\partial x}\left(\nu h\frac{\partial v}{\partial x}\right) + \frac{\partial}{\partial y}\left(\nu h\frac{\partial v}{\partial y}\right) \end{pmatrix}, \quad (19a)$$

$$\mathbf{X}_{(2)} = \begin{pmatrix} 0 \\ -ghun^2\frac{\sqrt{u^2+v^2}}{h^{4/3}} \\ -ghvn^2\frac{\sqrt{u^2+v^2}}{h^{4/3}} \end{pmatrix}. \quad (19b)$$

The solution of equation (18) can be split into two stages. In the first step equation

$$\mathbf{U}_{(1)}^{n+1} = \mathbf{U}_{(1)}^{n} + \int_0^{\Delta t} \mathbf{X}_{(1)}\, dt \quad (20)$$

with the initial condition $\mathbf{U}_{(1)}{}^n = \mathbf{U}^n$ should be solved. Then, in the second step, equation

$$\mathbf{U}_{(2)}^{n+1} = \mathbf{U}_{(2)}^{n} + \int_0^{\Delta t} \mathbf{X}_{(2)}\, dt \quad (21)$$

with the initial condition $\mathbf{U}_{(2)}{}^n = \mathbf{U}_{(1)}{}^{n+1}$ must be computed. The solution searched for at time $t+\Delta t$ is $\mathbf{U}^{n+1} = \mathbf{U}_{(2)}^{n+1}$. For SWE (1) in the first step all terms except for bottom friction term are integrated in time. In the second one only that term is taken into account. It can be seen, considering equations (19b) and (21), that only discharges ($qx=u\cdot h$, $qy=v\cdot h$) are modified at the second stage. Applying FDM implicit in time, the scheme to solve equation (21) in given cell i two formulas can be written

$$\frac{qx_{(2)i}^{n+1} - qx_{(1)i}^{n+1}}{\Delta t} = -g\, qx_{(2)i}^{n+1} n^2 \frac{\sqrt{\left(qx_{(2)i}^{n+1}\right)^2 + \left(qy_{(2)i}^{n+1}\right)^2}}{\left(h_{(2)i}^{n+1}\right)^{7/3}}, \quad (22a)$$

$$\frac{qy_{(2)i}^{n+1} - qy_{(1)i}^{n+1}}{\Delta t} = -g\, qy_{(2)i}^{n+1} n^2 \frac{\sqrt{\left(qx_{(2)i}^{n+1}\right)^2 + \left(qy_{(2)i}^{n+1}\right)^2}}{\left(h_{(2)i}^{n+1}\right)^{7/3}}, \quad (22b)$$

where superscripts n and $n+1$ denote previous and the next time level on numerical grid, respectively, and subscripts (1) and (2) represent first and second

integration step. Division of equations (22a, b) by $qx_{(2)i}^{n+1}$ and, $qy_{(2)i}^{n+1}$ respectively, yields

$$\frac{qx_{(1)i}^{n+1}}{qx_{(2)i}^{n+1}} - 1 = K_{(2)i}, \quad \frac{qy_{(1)i}^{n+1}}{qy_{(2)i}^{n+1}} - 1 = K_{(2)i} \tag{23a, b}$$

where

$$K_{(2)i} = g\Delta t n^2 \frac{\sqrt{\left(qx_{(2)i}^{n+1}\right)^2 + \left(qy_{(2)i}^{n+1}\right)^2}}{\left(h_{(2)i}^{n+1}\right)^{7/3}}. \tag{24}$$

Imposing

$$\alpha = \frac{qx_{(2)i}^{n+1}}{qx_{(1)i}^{n+1}} = \frac{qy_{(2)i}^{n+1}}{qy_{(1)i}^{n+1}} \tag{25}$$

equation (24) can be rewritten as

$$K_{(2)i} = \alpha K_{(1)i}. \tag{26}$$

Both equations (23a, b) together with (26) can be written in the quadratic equation form

$$K_{(1)i}\alpha^2 + \alpha - 1 = 0. \tag{27}$$

Finally, the second step of time integration procedure (21) is reduced to discharges correction

$$qx_{(2)i}^{n+1} = \alpha qx_{(2)i}^{n} = \alpha qx_{(1)i}^{n+1} \tag{28a}$$

$$qy_{(2)i}^{n+1} = \alpha qy_{(2)i}^{n} = \alpha qy_{(1)i}^{n+1} \tag{28b}$$

where $\alpha \in \langle 0,1 \rangle$ is no-negative root of equation (27). For no bottom friction case the coefficient α is equal to unity ($n = 0$). When bottom roughness exists ($\alpha < 1$) the absolute values of discharges qx and qy decrease. Thanks to this technique the bottom friction together with supercritical water flow can be taken into consideration. A similar procedure of friction term integration was presented by Paquier (1995). The good properties of the method were also reported by Szydłowski (1998).

6. Time Integration Scheme and Stability Condition

In order to complete the solution of equation (7) a numerical scheme solving equation (20) must be implemented. The general time integration scheme can be written as

$$\mathbf{U}^{n+1} = \mathbf{U}^n + \Delta t \left(\Theta \mathbf{X}^{n+1} + (1-\Theta)\mathbf{X}^n\right) \tag{29}$$

where superscripts n and $n+1$ denote previous and next time level on the numerical grid. When $\Theta=0$ equation (29) is the Euler explicit scheme and when $\Theta=1$

it is the Euler implicit scheme. For Θ=0.5 formula (29) becomes the well known trapezoidal implicit scheme. In the present work the two-step explicit scheme is used

$$\mathbf{U}^p = \mathbf{U}^n + 0.5\Delta t \mathbf{X}^n, \tag{30a}$$

$$\mathbf{U}^{n+1} = \mathbf{U}^n + \Delta t \mathbf{X}^p. \tag{30b}$$

This explicit scheme is of second-order accuracy in time and its stability is restricted by the Courant number. For 2D shallow water equations the stability condition can be written as (Potter 1977)

$$Cr = \frac{\max\left(\sqrt{u_i^2 + v_i^2} + \sqrt{g\,h_i}\right)}{\min\left(d_r\right)/\Delta\, t} \leq \frac{1}{\sqrt{2}} \tag{31}$$

where subscript i denotes the given cell and d_r represents the distances between centre points of cell i and its neighbouring volumes.

7. Boundary Conditions

A consistent set of initial and boundary condition is required to complement SWE (1). All conditions must be imposed in accordance with the characteristics theory. To start the computation the initial values of water depth and both components of velocity must be known inside every finite volume at time t=0. To impose the proper set of boundary conditions only the hyperbolic part of SWE (without the eddy viscosity term) can be considered and solved in boundary regions. Generally, the boundary of the computational domain is composed of solid and open segments. In the case of solid boundary the free-slip condition can be imposed. This means that the normal to cell-interface velocity component, as well as a derivative of tangential one in the same direction, should be set equal to zero. In the FVM there is no possibility to set any function value exactly at the boundary. This is impossible because the grid nodes are located in cell-centre points (Fig. 3).

To impose the boundary conditions correctly, the corresponding fluxes at this boundary must be computed. In order to calculate the numerical flux through the boundary of the computational domain, the virtual cell j (Fig. 3) can be defined. For closed boundaries the flow variables values should be imposed at node j (outside the domain) as follows

$$h_j = h_i,\ un_j = -un_i,\ us_j = us_i \tag{32a, b, c}$$

where h is the water depth and un and us denote the normal and tangential to boundary velocity component. Using the states $\mathbf{U}_i$ and $\mathbf{U}_j$ the flux through the cell-interface can be computed by Roe procedure.

At the open boundary the situation is more complex and needs to be treated in particular. In accordance with the characteristics theory, the number of conditions

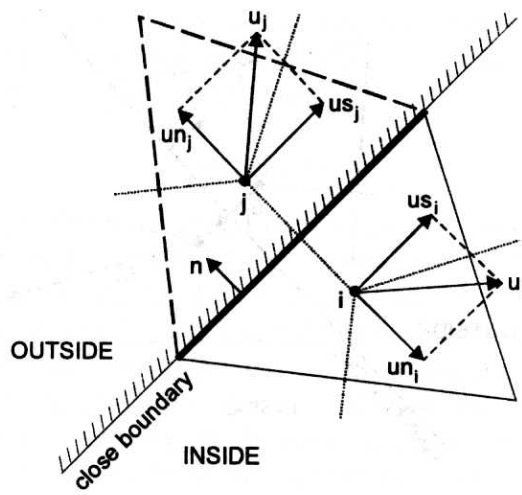

Fig. 3. The boundary cells (real i and virtual j) and velocity vectors for solid wall boundary condition

imposing at the boundary depends on the local value of Froude number and flow direction. The four cases at the open boundary must be considered (Tan 1992)

1. *supercritical inflow*
   All characteristics "enter" the calculation domain, so three conditions must be imposed (water depth and both velocity components).
2. *supercritical outflow*
   All characteristics "come out" of the calculation domain, so no condition is needed.
3. *subcritical inflow*
   Two characteristics "enter" the calculation domain, so two conditions must be imposed. In the present work the components of the normal to boundary velocity are chosen.
4. *subcritical outflow*
   Only one characteristic "enters" the calculation domain, so only one condition is required at the boundary. Here the water depth is chosen.

The conditions at the open boundary can be imposed in a manner similar to the procedure adopted for the closed boundary. First, virtual cell j outside the computational domain should be defined (Fig. 4). To obtain the fluxes at the boundary cell-interface, the state $\mathbf{U}_j$ inside cell j must be computed. When this is known all fluxes can be determined by the Roe scheme. For supercritical flow there is no difficulty in imposing the function values inside the exterior cell. It is more complicated for subcritical flow. In the case of subcritical inflow only two functions are known from boundary conditions (for example the normal velocity

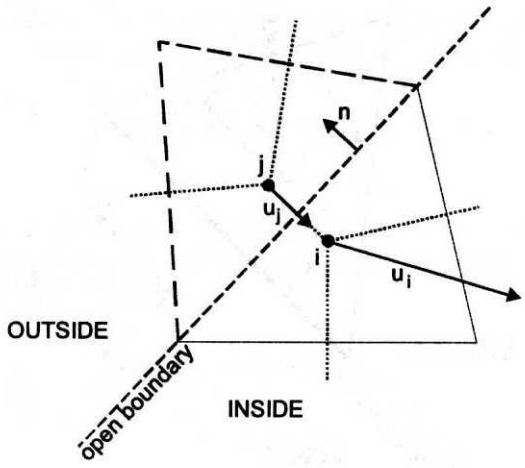

Fig. 4. The boundary cells (real i and virtual j) and velocity vectors for the open boundary condition

un_j components). The third one (water depth h_j) must be determined in an other way. It can be obtained using the Riemann invariant (Tan 1992)

$$un_j - 2\sqrt{gh_j} = R_i \tag{33}$$

where R_i is the value of the Riemann invariant computed basing on known values from cell i. In the same manner the subcritical outflow can be treated. In that case only one function value (for instance water depth h_j) is known from the boundary condition outside the calculation domain. The others can be estimated using the Riemann invariant

$$un_j + 2\sqrt{gh_j} = R_i \tag{34}$$

where R_i is determined by function values from interior cell i.

8. Numerical Results

First, in order to validate the inviscid part of SWE three test cases are presented. The results of simulation of one-dimensional dam-break flow over wet and dry bottoms are compared to analytical solutions of Saint-Venant equations (Stocker 1957, Ritter 1892). Unfortunately, this kind of solution does not exist for two-dimensional flow. Because of that computed water depth and velocities for 2D dam-break flow are compared with results presented by other authors (Fennema and Chaudhry 1990, Glaister 1993, Ambrosi 1995). The aim of the next tests is to examine the numerical computation against the experimental, measured data. First, the results reported by Bechteler et al. (1992) are considered. The physical modelling results used in the next two test cases are the effect of experimental work undertaken by the research group at the Hydraulic Laboratory of the Catholic University of Louvain (Soares 1997). For each test the computed results are

compared with the water level observed at gauging points. In order to evaluate the capacity of a numerical model to reproduce the eddy viscosity effects the test case reported by Stelling (1984) is examined.

Test Case No. 1

One-dimensional flow due to idealized dam-break is studied in this test. In the rectangular, 1.0 m wide and 400.0 m long -200.0 m $< x <$ 200.0 m channel two different water levels are separated by a gate located at $x = 0.0$ m. There is no bottom friction in the channel, water is initially at rest and bottom slope is equal to zero. The water levels are equal to 6.0 m and 1.0 m upstream and downstream of the gate, respectively. After sudden removal of the gate the water is released and the wave propagates downstream. At the same time a negative wave spreads into the upstream channel. During the simulation the waves do not reach the domain boundaries. The water flow was simulated using a one-dimensional version of the numerical scheme presented (Szydłowski 1998). The channel was discretized with 800 cells (Δx=0.5 m) and all calculations were carried out with the time step Δt=0.01 s.

Test Case No. 2

The simulation was run under the same conditions as the previous one, with the except of the water level downstream of the gate. In this case the channel bottom is covered by a 10^{-5} m thick water film.

The numerical and analytical solutions (Stoker 1957; Ritter 1892) after t=10 s for *tests nos* 1 and 2 are presented in Figures 5 and 6, respectively. The numerical solution gives a good representation of exact one in both cases, except for the contact wet-dry bottom region in *test* 2 where disagreement of velocities and Froude numbers is observed (Fig. 6b, d). For supercritical flow (when the upstream and downstream water depth ratio is relatively large) the mesh should be refined to obtain better agreement between the numerical and analytical solution. The disagreement in *test* 2 is also caused by the fact that the "dry bottom" is the zone covered by the water film, as the Ritter solution is obtained for a depth equal to zero.

Test Case No. 3

Two-dimensional flow due to dam-break is studied. The geometry of the computational domain is presented in Fig. 7. The domain is composed of a 200.0 m long and 200.0 m wide basin and dam with 75.0 m long non-symmetrical breach. There is no bottom friction in the basin and the bottom slope is equal to zero. At time t=0 s the water is at rest and there are two different water levels on each side of the dam. The water depth is equal to 10.0 m and 5.0 m in the upstream and

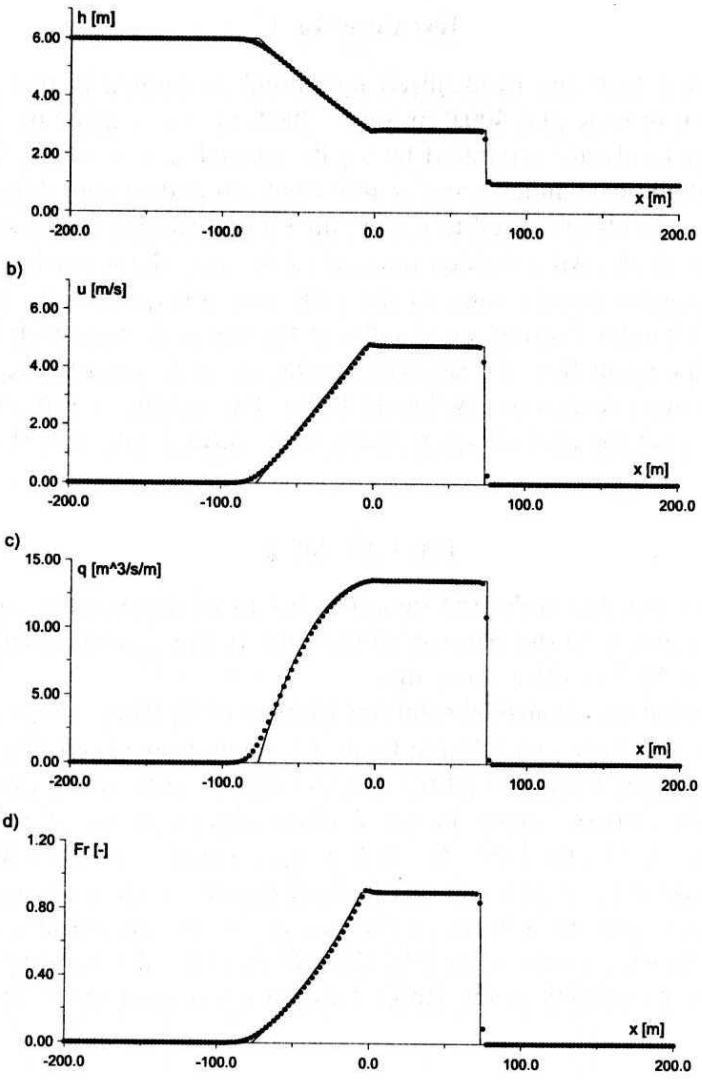

Fig. 5. Test 1 – numerical (•) and analytical (–) Stoker (1957) solution after $t=10$ s; a) water level, b) velocity, c) discharge, d) Froude number

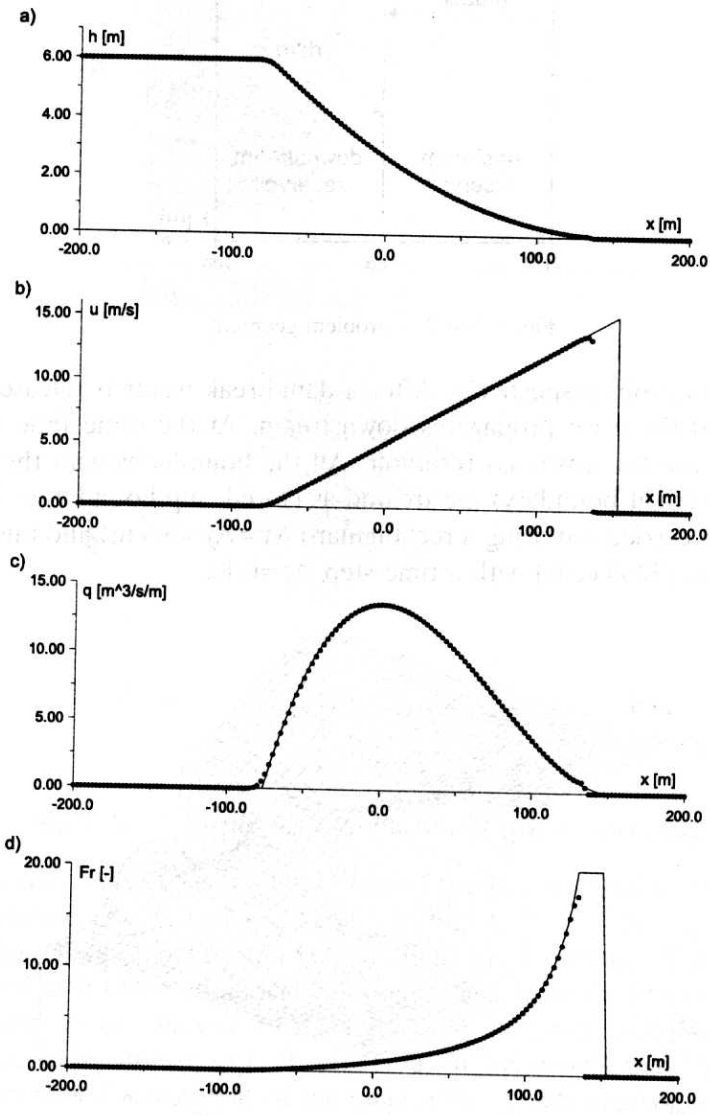

Fig. 6. Test 2 – numerical (•) and analytical (–) Ritter (1892) solution after $t=10$ s; a) water level, b) velocity, c) discharge, d) Froude number

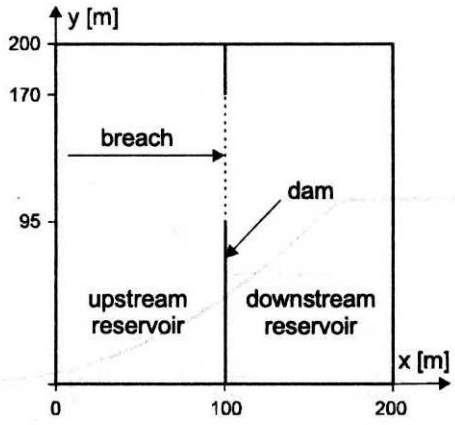

Fig. 7. Test 3 – problem geometry

downstream reservoir, respectively. After a dam-break water is released through the breach and the wave propagates downstream. At the same time a negative wave spreads into the upstream reservoir. All the boundaries with the exception of the outflow (right boundary) are treated as closed, slip boundaries. Numerical simulation was carried out using a rectangular ($\Delta x = \Delta y = 5.0$ m) and unstructured, triangular mesh (3280 cells) with a time step $\Delta t = 0.1$s.

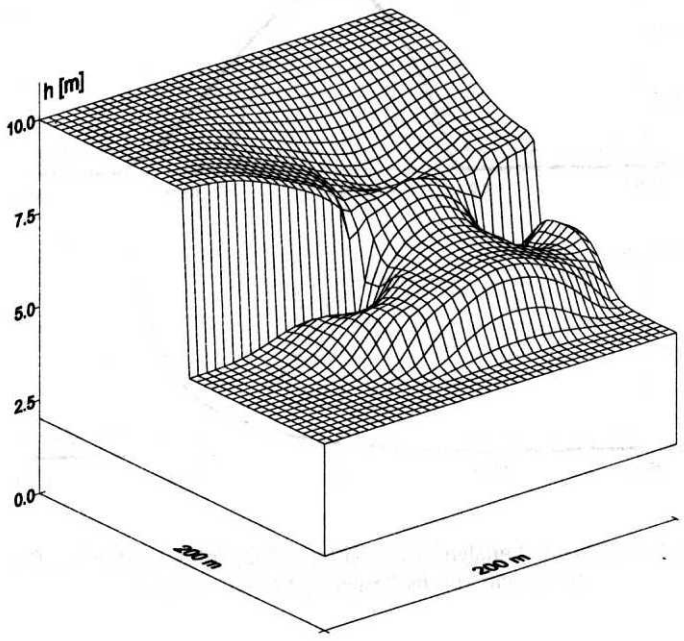

Fig. 8. Test 3 – water surface after $t = 7.2$ s

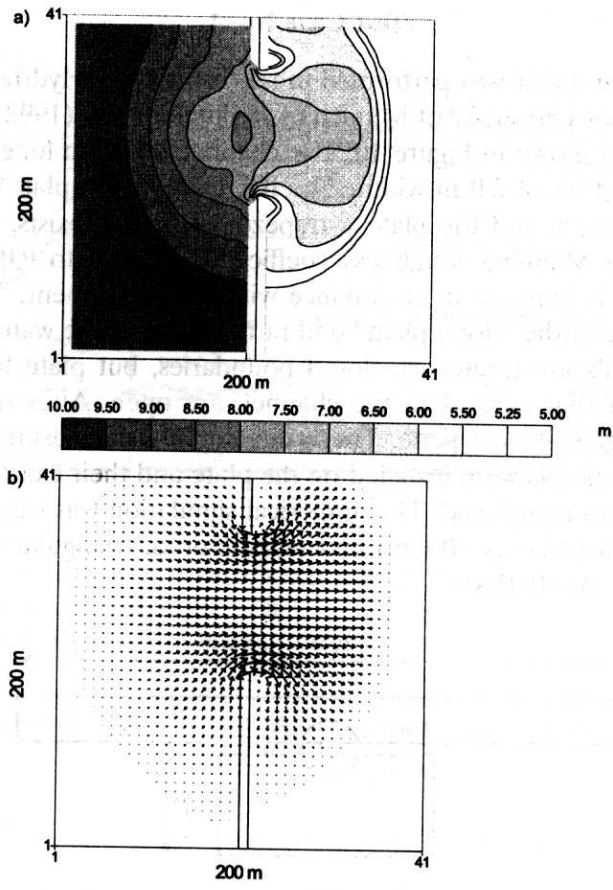

Fig. 9. Test 3 – water depth (a) and velocity field (b) after t=7.2 s

The results obtained using both kinds of mesh were similar. The carpet plot of water surface after t=7.2 s is shown in Figure 8. In Figures 9a and 9b the contour plot of water depth and velocity field are presented. These results can be compared with other numerical solutions available in the literature (Fennema and Chaudhry 1990, Glaister 1993, Nujic 1995, Ambrosi 1995). The computed results seem to be similar to each other but unfortunately that kind of graphic presentation makes assessment of the quantitative result impossible.

Test Case No. 4

The physical experiment was performed in the Institute of Hydrosciences of Federal Armed Forces University of Munich by Bechteler et al. (1992). The geometry of the problem is shown in Figure 10. The channel is 30.0 m long and has a rectangular cross section of 2.0 m width. The flat plate (flood plain) is 5.0×10.0 m. Between the channel and the plate a trapezoidal breach exists, which is closed with a flap. The Manning roughness coefficient is equal to 0.01 $m^{-1/3}$ s. The initial condition is imposed in accordance with the experiment. This means that there is no water in the "flood plain" and in the channel the water is 0.2 m deep. The channel walls are treated as closed boundaries, but plate boundaries, with the exception of that parallel to the channel, are open. After opening the flap the wave propagates to the plate. The water depth was measured at 29 gauging points. All these points were installed on the plate and their exact location can be found in the paper mentioned. The numerical simulation was carryied out using a rectangular mesh ($\Delta x=\Delta y=0.1$ m) and unstructured, triangular one (3866 cells) with a time step $\Delta t=0.01$ s.

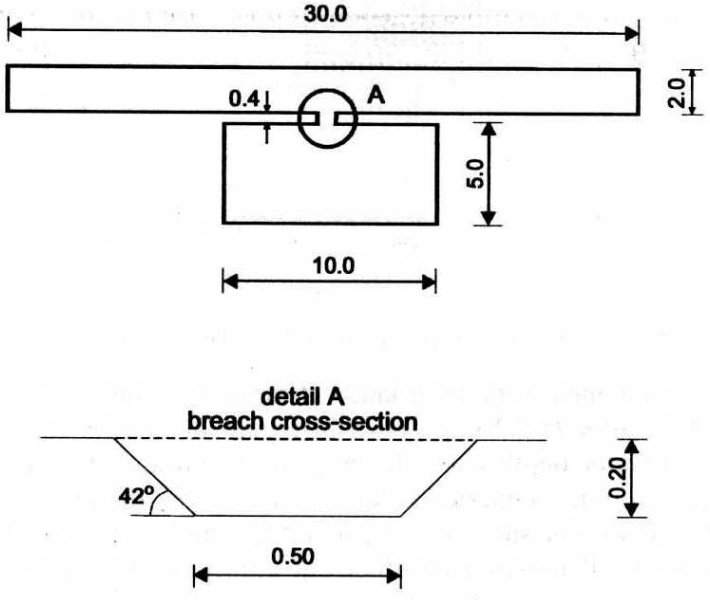

Fig. 10. Test 4 – problem geometry (all dimensions in metres)

The results obtained were very similar therefore, only the first are presented in this paper. Two different tests were performed by Bechteler's group. First, the flood wave on the horizontal plate was simulated. In the second test an inverse slope (1.8 degrees) of the plate was implemented. The computed and measured results for both tests are shown in Figures 11 and 12, respectively. The gauging

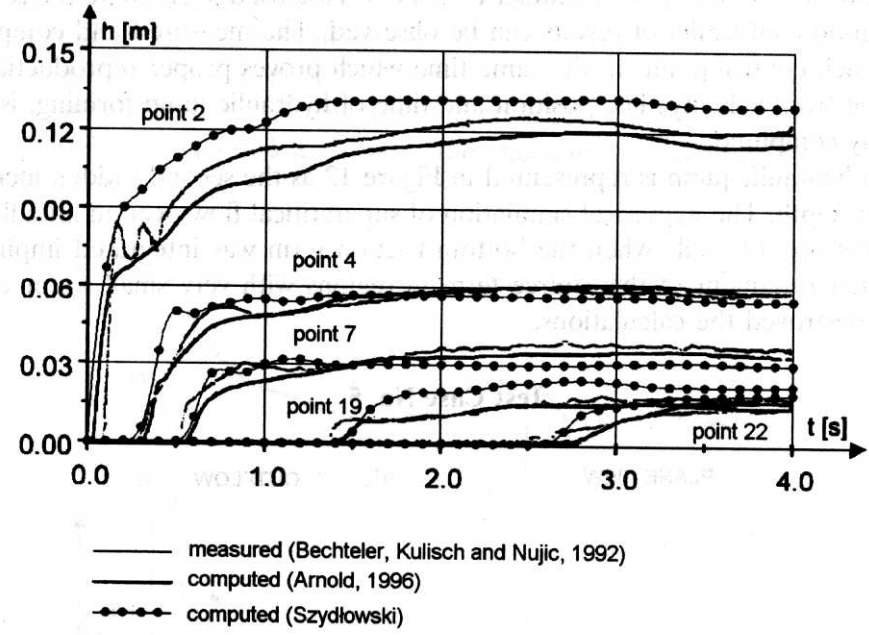

Fig. 11. Test 4 – computed and measured hydrographs (horizontal plate)

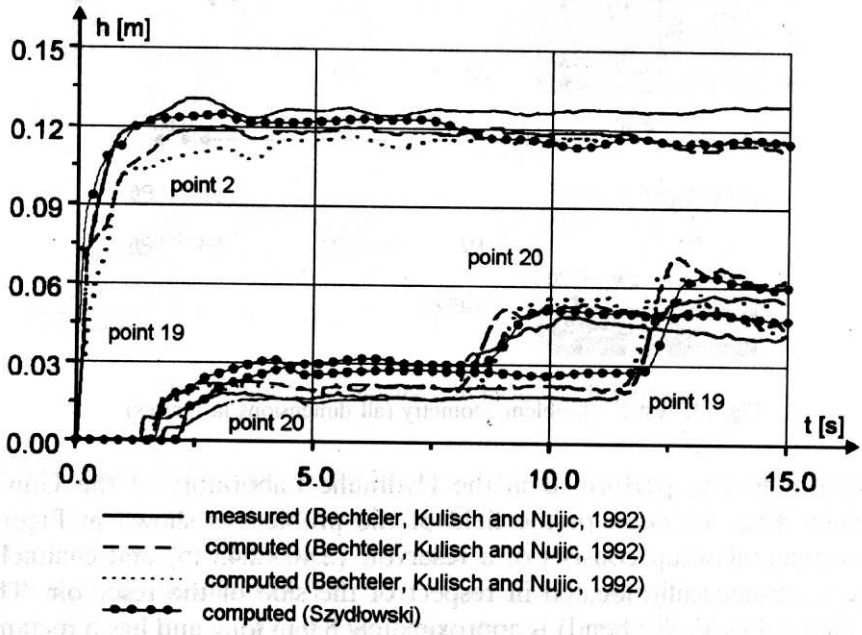

Fig. 12. Test 4 – computed and measured hydrographs (increasing plate)

points previously chosen by Bechteler et al. (1992) are used to compare the results. Quite good conformity of results can be observed. The measured and computed wave reach control points at the same time which proves proper reproduction of the wave front velocity. The position and time of hydraulic jump forming, is also correctly computed.

The hydraulic jump is represented in Figure 12 as the second sudden increase in water depth. The numerical simulation of supercritical flow over an initially dry plate was possible only when the bottom friction term was integrated implicitly. The other treatment of this source term in regions with very small water depth always destroyed the calculations.

Test Case No. 5

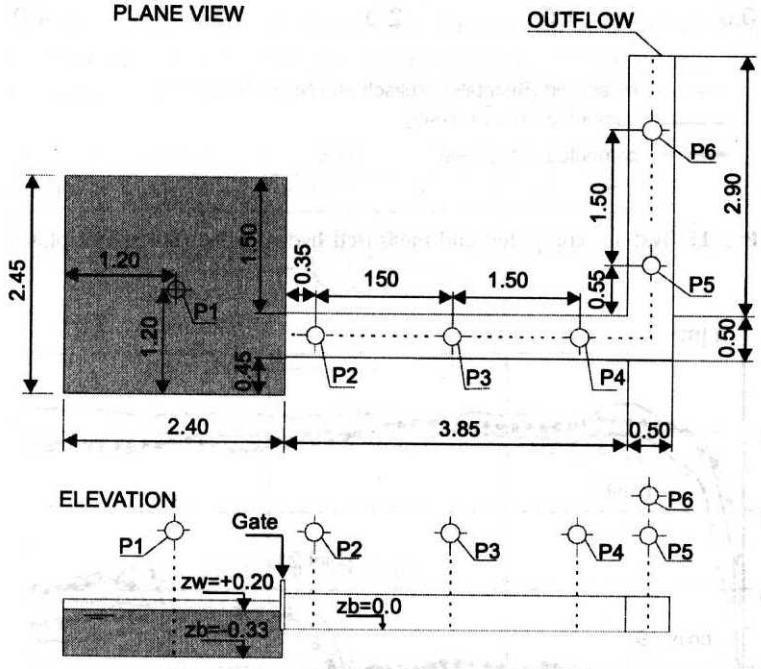

Fig. 13. Test 5 – problem geometry (all dimensions in metres)

This experiment was performed in the Hydraulic Laboratory of the University of Louvain. The definition of the field of the problem is shown in Figure 13. The experimental setup consists of a reservoir (2.40×2.45 m) and channel with entrance asymmetrically located in respect of the side of the reservoir. The L-shaped channel (with 90° bend) is approximately 8.0 m long and has a rectangular cross section 0.5 m in width. The channel bottom is 0.33 m above the bottom of the reservoir, therefore, an abrupt step at the channel entrance is present. The

Manning coefficient is equal to 0.0095 $m^{-1/3}s$. The reservoir and channel are separated by the gate. The initial condition is imposed in accordance with the experiment. The water level in the reservoir is 0.20 m above the channel bottom and the water is at rest. The channel bottom is covered by a 0.01 m water film. The reservoir and channel walls, with the exception of outflow, are treated as closed boundaries.

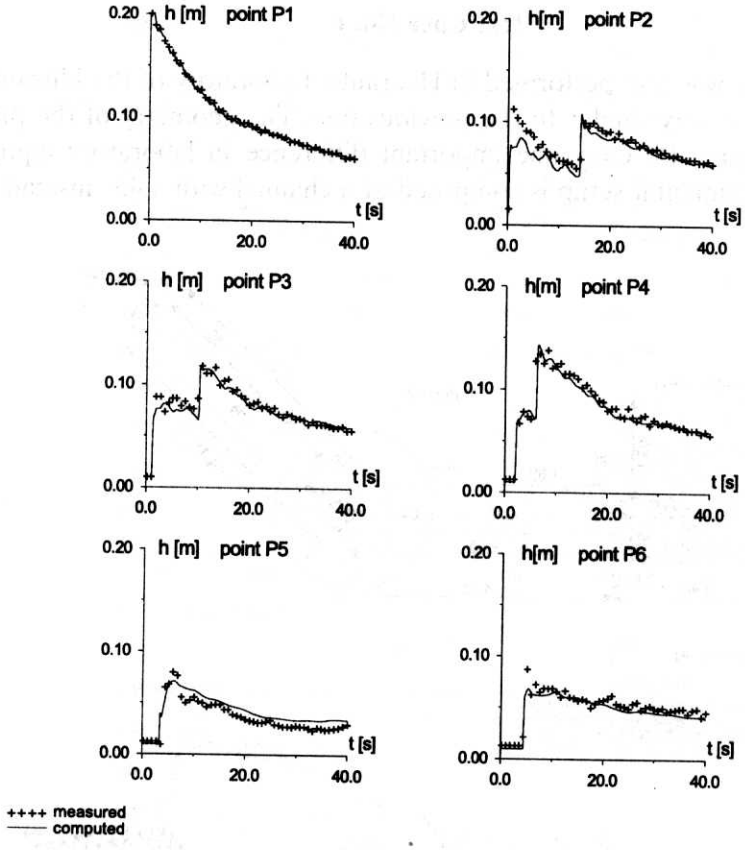

Fig. 14. Test 5 – computed and measured hydrographs

After removing the gate, water is released and the wave passes downstream. At the same time, a negative wave spreads into the upstream reservoir. One of the water level measure points (P1) is in the centre of the reservoir and the others are located along the channel. The water flow was simulated on rectangular mesh ($\Delta x = \Delta y = 0.05$ m) and unstructured, triangular one (2124 cells) with a time step of $\Delta t = 0.01$ s. The obtained results were similar, so only these first are presented here.

The computed and measured hydrographs are shown in Figure 14. Consistent results were obtained. The calculated wave front has the proper velocity and the hydraulic jump, formed after water reflection in the channel corner, appears where it is expected. The negative wave (Fig. 14a, point P1) is also in good conformity with the experiment. No calculation difficulties in the region of abrupt bottom step were observed during numerical simulation. This good calculation scheme property proves the appropriate bottom slope term approximation.

Test Case No. 6

This experiment was also performed in Hydraulic Laboratory of the University of Louvain and it is very similar to the previous one. The geometry of the problem is shown in Figure 15. Only one important difference in laboratory equipment exists. The experimental setup is composed of a channel with a 45° instead of 90° bend.

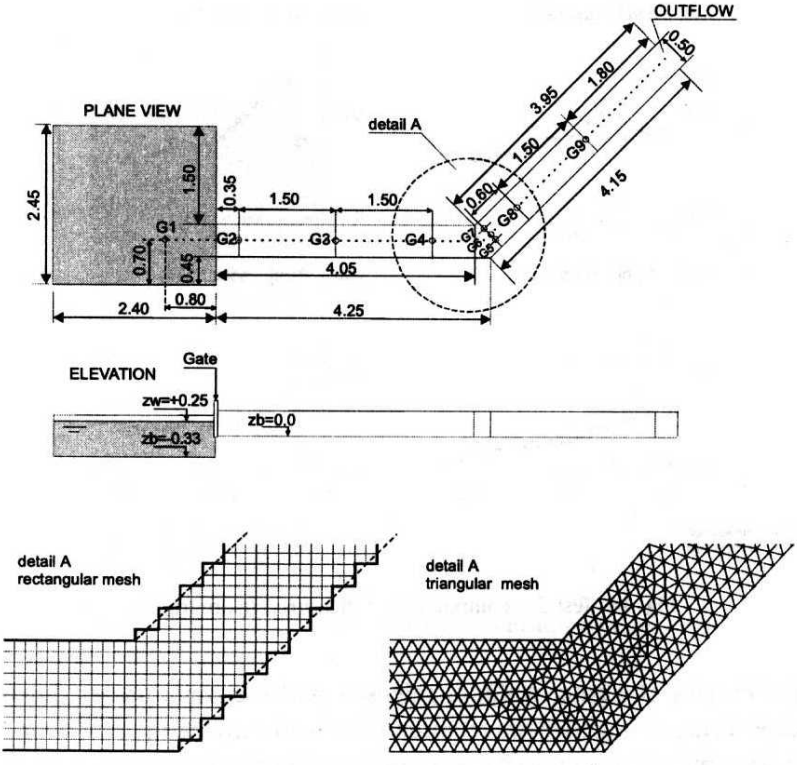

Fig. 15. Test 6 – problem geometry (all dimensions in metres)

The experiment is run with the same conditions as the previous one, except for the water level in the reservoir. In this case the water surface is 0.25 m above

the channel bottom. The gauging points are located along the channel and G1 is in front of the channel entrance.

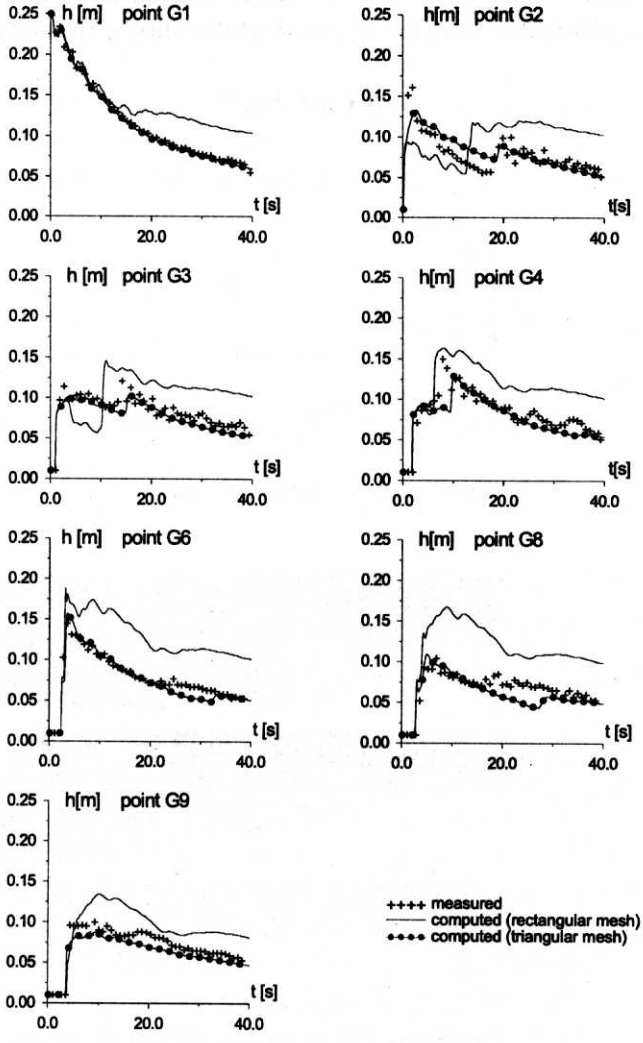

Fig. 16. Test 6 – computed and measured hydrographs

Numerical simulation was carried out using a rectangular mesh ($\Delta x = \Delta y =$ 0.05 m) and unstructured, triangular one (2346 cells) with time step Δt=0.01 s. The results obtained for both meshes differ greatly from each other. The computed and measured hydrographs are shown in Figure 16. The results calculated on rectangular mesh are inconsistent with the experimental data. The hydraulic jump formed in the channel bend and moving upstream is stronger than that observed. This unexpected effect is the result of poor boundary approximation in the band

region (Fig. 15). The conditions imposed at the stepped-line boundary generate the spurious, unphysical results. To avoid this undesired boundary influence, the geometry of calculation domain is approximated by unstructured mesh. The results calculated using triangular cells are in good conformity with measurements.

Test Case No. 7

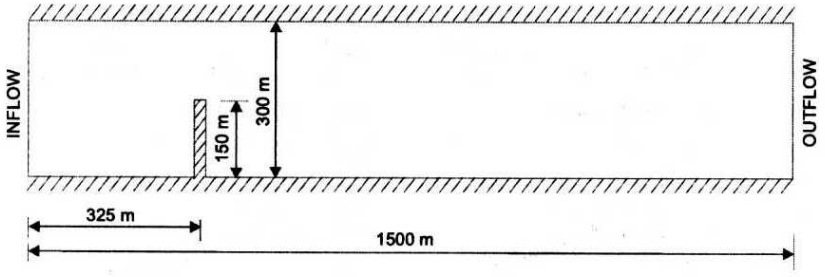

Fig. 17. Test 7 – problem geometry

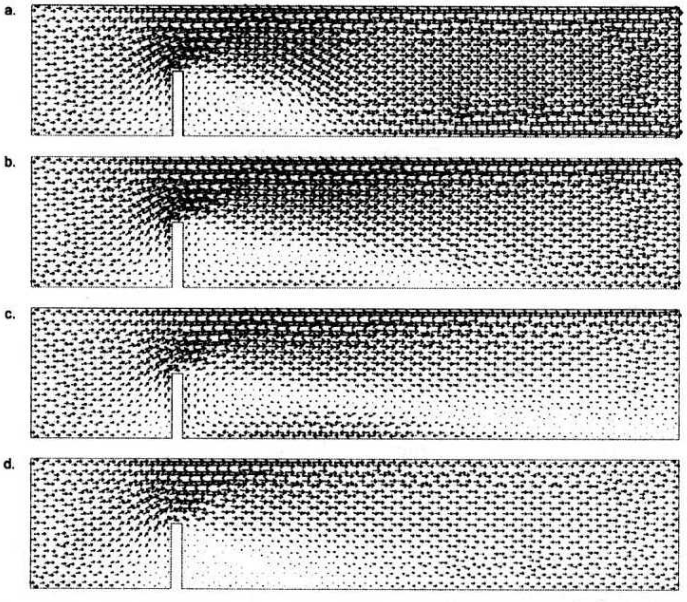

Fig. 18. Test 7 – flow fields after 10, 30, 180 s for inviscid flow (a, b, c) and after 60 s for viscid flow (d)

In order to validate the full SWE, including the eddy viscosity term, the numerical test reported by Stelling (1984) is studied. The geometry of computational domain

is shown in Figure 17. The channel (basin) is 1500 m long and has a width of 300 m. The 150 m long jetty is located 325 m from the left boundary of the domain. The Manning coefficient is set equal to 0.026 $m^{-1/3}$ s. Initially, the water is at rest and the depth in whole channel is 25 m. The boundary conditions are imposed as uniform velocity of 0.5 m/s at the left boundary and constant water depth 25 m at the right one. These conditions produce a steady state problem during water flow simulation. The numerical calculation was carried out using triangular mesh (1654 cells) with the time step Δt=0.25 s.

The results of calculation are presented in Figure 18. The flow fields shown in Figures 18a, b, c represent the velocity evolution of inviscid flow. The length of eddy, behind the jetty, grows and the steady state is reached very slowly. It can be observed after t=180 s (Fig. 18c). The computed results for viscid flow (eddy viscosity coefficient set equal to 10) are shown in Figure 18d. The eddy is shorter than in the previous simulation and the steady state is formed quicker. It can be observed already after t = 60 s. The results presented are in good qualitative agreement with those obtained by Stelling.

9. Conclusion

The finite volume method based on unstructured, triangular mesh for SWE was studied. The numerical scheme, presented in this paper, can be used to solve shallow water equations for both rapidly and gradually varied flow. The numerical solution for the first kind of flow posed four main difficulties. It had to handle the discontinuities (wave fronts, hydraulic jumps) and provide an accurate solution for flow over a abrupt bottom. These two aims were ensured by applying the Roe idea of numerical fluxes and Bermudez and Vazquez idea of numerical sources, respectively. The importance of adequate computational domain representation was underlined. For some cases, the poor geometry approximation (rectangular mesh) produced unexpected, unphysical results. These numerical errors were caused by improper boundary condition imposing. There is no possibility of imposing the proper physical condition on rectangular mesh at every segment of the complex boundary. To improve the computations, the triangular, unstructured mesh was implemented. This kind of numerical mesh ensures the consistence of mathematical and physical boundary conditions and the flexibility of domain approximation. Even complex boundaries can be precisely represented by triangular cells. Therefore, thanks to these properties, the finite volume method based on triangular cells has the advantage of FEM keeping clarity of FDM. The fourth numerical difficulty, the instability of SWE numerical solution due to bottom friction term integration, was avoided by splitting technique. The water flow equations were split with respect to physical processes. This approach reduced the time integration of inconvenient source term to simple discharge correction. In order to simulate the gradually varied flow the full SWE should be solved. The viscid terms included in

SWE were integrated in a manner consistent with the finite volume method. Necessary function derivatives were approximated as in FEM. The numerical results of water flow simulation were compared with some analytical solutions, experimental data and results available in the literature. Generally, for rapidly and gradually varied flow good conformity between these results was observed. The numerical model produced sufficiently accurate results for advection dominated problems, e.g. the dam-break flood flows and properly reproduced eddy viscosity effects. The good properties of the numerical scheme presented and satisfactory computational results proved the effectiveness of the proposed method for both rapidly and gradually varied water flow.

References

Abbott M. B. (1979), *Computational hydraulics: elements of the theory of free-surface flows*, Pitman, London.

Ambrosi D. (1995), Approximation of shallow water equations by Roe's Riemann solver, *Int. Journal for Numerical Methods in Fluids*, Vol. 20, 157–168.

Arnold H. (1996), *Simulation Dammbruchinduzierter Flutwellen*, Univeristät Hannover, Bericht No. 46/1996.

Bechteler W., Kulisch H., Nujic M. (1992), 2D dam-break flooding waves – comparison between experimental and calculated results, 3*rd Int. Conference on Flood and Flood Management*, Florence, 24–26.

Bermudez A. and Vazquez M. E. (1994), Upwind methods for hyperbolic conservation laws with source terms, *Computers and Fluids*, 23, 1049–1071.

Bronsztejn I. N., Siemiendiajew K. A. (1973), *Matematyka – Poradnik encyklopedyczny*, PWN, Warszawa.

Cunge J. A., Holly Jr F. M., Verwey A. (1980), *Practical Aspects of Computational River Hydraulics*, Pitman, London.

Fennema R. J., Chaudhry M. H. (1990), Explicit methods for 2-D transient free-surface flows, *Journal of Hydraulic Engineering*, Vol. 116, No. 3, 1013–1034.

Glaister P. (1993), Flux difference splitting for open-channel flows, *Int. Journal for Numerical Methods in Fluids*, Vol. 16, 629–654.

Goutal N., Maurel F. (Editors) (1997), *Proceedings of the 2nd workshop on dam-break wave simulation*, EDF Internal Rapport HE–43/97/016/B.

Jha A. K., Akiyama J., Ura M. (2000), Flux-Difference Splitting Schemes for 2D Flood Flows, *Journal of Hydraulic Engineering*, Vol. 126, No. 1, 33–42.

Katopodes N. D. (1984), A dissipative Galerkin scheme for open channel flow, *Journal of Hydraulic Engineering*, Vol. 110, No. 6, 450–466.

Nujic M. (1995), Efficient implementation of non-oscillatory schemes for the computation of free-surface flows, *Journal of Hydraulic Research*, Vol. 3, No. 1.

Paquier A. (1995), *Modelisation et simulation de la propagation de l'onde de rapture de barrage*, These de l'Universite Jean Monnet, St. Etienne.

Potter D. (1977), *Metody obliczeniowe fizyki*, PWN, Warszawa.

Ritter A. (1892), Die Fortplanzung der Wasserwellen, *Zeitschrift des Vereines Deutscher Ingeniere*, 33(36), 947–954.

Roe P. L. (1981), Approximate Riemann solvers, parameters vectors and difference schemes, *Journal of Computational Physics*, 43, 357–372.

Sa da Costa A., Batista Melo A., Gray W. G., Brebbia C. A., Pider G. F. (Editors) (1986), *Finite elements in water resources*, Proc. 6th Int. Conf. in Lisboa, Springer-Verlag, Berlin.

Sawicki J. (1998), *Przepływy ze swobodną powierzchnią*, PWN, Warszawa.

Soares S. (Editor) (1997), *Proceeding of 3rd Workshop of Working Group on Dam-Break Modelling*, 23 and 24 June, Louvain-la-Neuve.

Steger J. L., Warming R. F. (1981), Flux-vector splitting of the inviscid gas dynamic equations with applications to finite-difference methods, *Journal of Computational Physics*, 40, 263–293.

Stelling G. S. (1984), *On the construction of computational methods for shallow water flow problems*, Rijkswaterstaat Communication, 35, Hague.

Stoker J. J. (1957), *Water Waves*, Interscience Publishers, Wiley, New York.

Szydłowski M. (1998), *Numeryczna symulacja przepływu wody ze swobodną powierzchnią w warunkach ruchu szybkozmiennego z nieciągłościami*, PhD thesis, Technical University of Gdańsk.

Szymkiewicz R. (1991), Finite-element method for the solution of the Saint Venant equations in an open channel network, *Journal of Hydrology*, Vol. 122, 275–287.

Szymkiewicz R. (1993), Oscillation-free solution of shallow water equations for nonstaggered grid, *Journal of Hydraulic Engineering*, Vol. 119, No. 10, 1118–1137.

Szymkiewicz R. (1995), *Method to solve 1D unsteady transport and flow equations*, Journal of Hydraulic Engineering, Vol. 121, No. 5, 396–403.

Tan W. (1992), *Shallow water hydrodynamics*, Elsevier, Amsterdam.

Toro E. F. (1997), *Riemann solvers and numerical methods for fluid dynamics*, Springer-Verlag, Berlin.

Zienkiewicz O. (1972), *The finite elements method*, Arkady, Warsaw.